APPLIED PHYSICS LETTERS **111**, 102101 (2017)

Variable range hopping electric and thermoelectric transport in anisotropic black phosphorus

Huili Liu,[1,2] Hwan Sung Choe,[2,3] Yabin Chen,[2] Joonki Suh,[2] Changhyun Ko,[2]
Sefaattin Tongay,[4] and Junqiao Wu[1,2,3,a)]
[1]*Materials Sciences Division, Lawrence Berkeley National Laboratory, Berkeley, California 94720, USA*
[2]*Department of Materials Science and Engineering, University of California, Berkeley, California 94720, USA*
[3]*Tsinghua-Berkeley Shenzhen Institute, University of California, Berkeley, California 94720, USA*
[4]*School for Engineering of Matter, Transport and Energy, Arizona State University, Tempe, Arizona 85287, USA*

(Received 30 May 2017; accepted 22 August 2017; published online 5 September 2017)

Black phosphorus (BP) is a layered semiconductor with a high mobility of up to ~1000 cm^2 V^{-1} s^{-1} and a narrow bandgap of ~0.3 eV, and shows potential applications in thermoelectrics. In stark contrast to most other layered materials, electrical and thermoelectric properties in the basal plane of BP are highly anisotropic. To elucidate the mechanism for such anisotropy, we fabricated BP nanoribbons (~100 nm thick) along the armchair and zigzag directions, and measured the transport properties. It is found that both the electrical conductivity and Seebeck coefficient increase with temperature, a behavior contradictory to that of traditional semiconductors. The three-dimensional variable range hopping model is adopted to analyze this abnormal temperature dependency of electrical conductivity and Seebeck coefficient. The hopping transport of the BP nanoribbons, attributed to high density of trap states in the samples, provides a fundamental understanding of the anisotropic BP for potential thermoelectric applications. *Published by AIP Publishing.* [http://dx.doi.org/10.1063/1.4985333]

As an advanced energy harvesting technology, thermoelectrics is playing an increasingly important role in modern energy application, because it directly converts thermal energy to electricity with no moving parts.[1] Thermoelectric materials are usually narrow bandgap semiconductors, such as Bi_2Te_3, PbTe, etc.[2] The heat-to-electricity energy conversion efficiency is a function of the dimensionless figure of merit, $zT = S^2\sigma T/\kappa$, where S is Seebeck coefficient, σ is electrical conductivity, T is absolute temperature, and κ is thermal conductivity of the material. Recent efforts have been focused on micro/nanostructuring of bulk materials to search for better thermoelectric materials,[3,4] because it is expected thermal conductivity can be reduced in low-dimensional materials when their size approaches the phonon mean free path, and their Seebeck coefficient may be also enhanced when the density of states is restructured by quantum confinement. The low dimensional materials, especially layer-structured two dimensional (2D) materials, such as transition metal dichalcogenides (TMDs), draw much attention in electronic applications.[5,6] In this context, these layered materials may also offer good thermoelectric properties, as their layer-structure may also be viewed as some kind of "natural nanostructuring." Black phosphorus (BP) is a rediscovered layered semiconductor. It is found that BP has a high mobility of up to ~1000 cm^2 V^{-1} s^{-1} (Ref. 7) and a narrow bandgap of ~0.3 eV (for thickness $\gtrsim$ 4 nm).[8] As a narrow bandgap semiconductor, BP has been evaluated for potential applications in 2D nanoelectronics.[9] It was reported that the Seebeck coefficient of BP is in the range of 335–415 μV/K at 300–385 K for the bulk,[10] and reaches 510 μV/K at 210 K with ion-gate tuning.[11] Theoretically, few-layer BP have been predicted to be a promising thermoelectric material with a high zT when under stress or doping.[12,13] More interestingly, BP is a strongly anisotropic material even in the basal plane: the thermal conductivity is much higher along the zigzag than the armchair direction, while electrical conductivity shows the opposite anisotropy.[14] Choi *et al.*[15] demonstrated that the variable range hopping (VRH) dominates electrical transport in thin BP flakes (10–30 nm thick). However, the BP flake crystal orientation was not specified in Choi and the coupling between the VRH process and the intrinsic anisotropy in BP is unclear. In this work, we elucidate and parameterize the VRH mechanism along the zigzag and armchair directions in BP. This was achieved by fabricating BP nanoribbons (thickness ~100 nm) along armchair and zigzag directions, respectively, and conducting temperature dependent measurements of electrical conductivity (σ) and Seebeck coefficient (S). Both σ and S increase as temperature rises, showing a behavior opposite to that of traditional semiconductors, which can be quantitatively explained by the VRH model. The hopping transport is attributed to existence of high density of trap states in the samples, which was further confirmed by artificially introducing more defects with high-energy particle irradiation.[16]

In BP, phosphorus atoms form a puckered honeycomb lattice with space group of Cmca (orthorhombic, $a = 3.316$ Å, $b = 10.484$ Å, $c = 4.379$ Å, $\alpha = \beta = \gamma = 90°$).[17] The schematic diagram of the crystal structure is shown in Fig. 1(a). A mechanically exfoliated BP flake is shown in Fig. 1(b), where the thickness is 100 (±2) nm conformed by atomic force microscopy (AFM). The crystallographic orientations of the flake were confirmed by micro-Raman analysis, as the Raman signal depends on the angle between the laser polarization direction and the BP crystal orientation.[18,19] Figures 1(c)–1(e)

[a)]Author to whom correspondence should be addressed: wuj@berkeley.edu

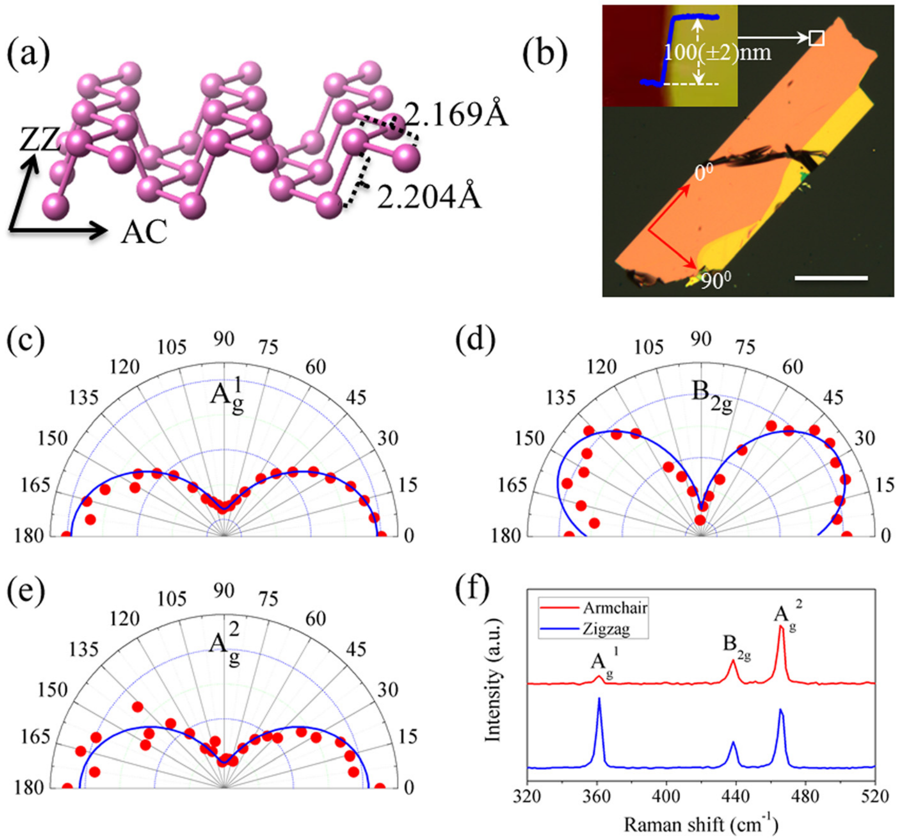

FIG. 1. Crystal structure and characterization of black phosphorus flakes. (a) Crystal structure: zigzag direction is paralleling to the atomic ridges and armchair perpendicular to atomic ridges; (b) optical image of a BP flake: 0° and 90° indicate the angle for Raman laser polarization directions. Inset is AFM image and height data, which show that the thickness of the flake is 100(±2) nm. The scale bar is 50 μm. (c)–(e) Angular dependence of intensity of typical Raman peaks for A_g^1 (361.4 cm^{-1}), B_{2g} (438.4 cm^{-1}), and A_g^2 (465.5 cm^{-1}). Solid lines are theoretical fitting results; (f) normalized intensity of BP flakes for Raman laser polarization at 0° and 90° in (b), indicating the crystal orientation: zigzag is parallel to 0° and armchair along 90°.

show the angular dependence of the intensity for the most prominent Raman peaks: A_g^1 (361.4 cm^{-1}), B_{2g} (438.4 cm^{-1}), and A_g^2 (465.5 cm^{-1}), which were fitted by the theoretically predicted angular dependences. Figure 1(f) shows the normalized (to A_g^2 mode) intensity of BP flakes.

BP nanoribbons were then fabricated with ~2 μm in width and ~35 μm in length using electron beam lithography. A second lithography was used to pre-deposit four-probe metal (Ti/Au) contacts onto each of the nanoribbons. Individual nanoribbon was then dry transferred to bridge two suspended pads[20] for reliable electrical and thermoelectric measurements. To further reduce the electric and thermal contact resistance, Pt metal was deposited onto the four-probe points with focused ion beam (FIB) to bond the pre-deposited metal contacts with the underlying metal electrodes [Fig. 2(h)]. During this process, the nanoribbons were minimally perturbed, such that any strain, bending, and twisting of the samples can be maximally avoided. The use

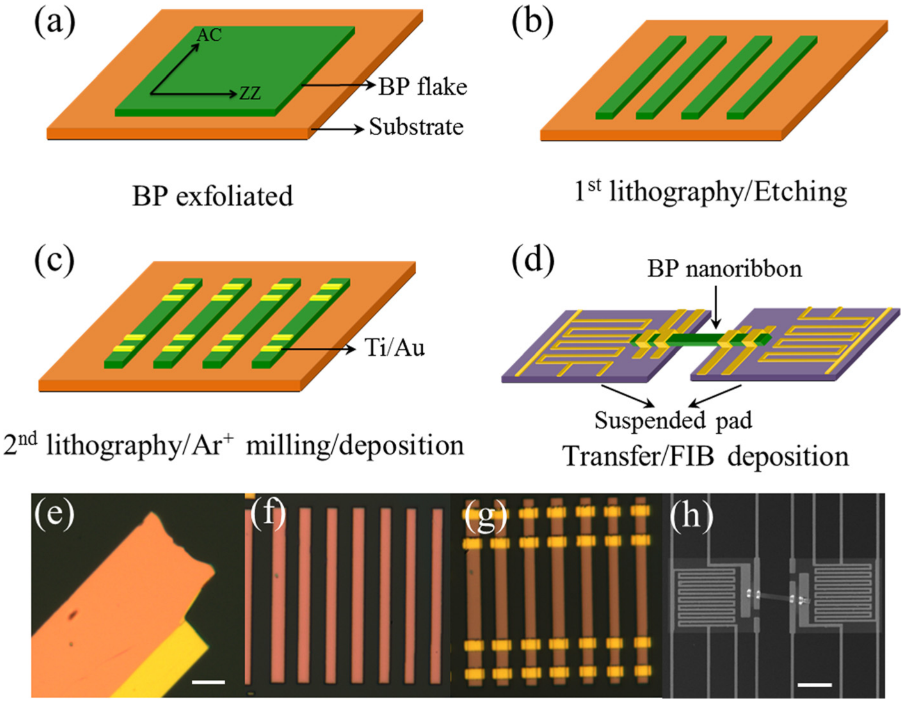

FIG. 2. Devices fabrication process. (a) BP exfoliated onto a SiO_2(250 nm)/Si substrate, then coated with PMMA; (b) the 1st electron beam lithography to tailor the nanoribbons; (c) the 2nd electron beam lithography to deposit Ti(10 nm)/Au(70 nm) contacts; (d) dry transfer BP nanoribbon onto suspended pads, and deposit Pt for bonding it onto electrodes using FIB; (e)–(g) optical images of BP flake, tailored nanoribbons, and nanoribbons with pre-deposited Ti/Au; (h) SEM image of BP nanoribbons device after transfer and FIB deposition. The scale bar is 20 μm in (e), (h).

of the suspended pads (as opposed to making devices directly on solid substrate[21]) helps to reduce any strain and substrate influence, as the nanoribbon body is suspended in vacuum and free to expand/shrink along its length direction. Moreover, the suspended pad method ensures a superior temperature control and sensing as heat leakage is minimized. Measurements using the suspended-pad method were described in previous reports.[20,22,23] All measurements were performed under low vacuum ($<10^{-6}$ Torr) with radiation shield. (See the details of devices fabrication process and measurements in supplementary material.)

Figures 3(a) and 3(c) show the temperature dependence of electrical conductivity and Seebeck coefficient of BP nanoribbons along the armchair and zigzag directions. Consistent with previous results,[14] these ribbons exhibit p-type conduction. The anisotropic ratio at room temperature is $\sigma_{AC}/\sigma_{ZZ} \sim 2.2$ and $S_{AC}/S_{ZZ} \sim 1.3$. As a comparison, the anisotropic ratio of mobility and effective mass was reported to be ~ 1.5 $(=\mu_{AC}/\mu_{ZZ})$[7] at 300 K and ~ 0.16 $(=m_{AC}/m_{ZZ})$,[24] respectively. The thermoelectric transport is not intrinsic from the native band structure of BP, and the anisotropy of Seebeck does not necessarily match the band transport scenario. In the Mott's picture, the Seebeck is dominated by the differentiation of the density of states with respect to energy at the Fermi level; therefore, the anisotropy of that differentiation is responsible for the anisotropic Seebeck coefficient in BP. Meanwhile, in traditional semiconductors, σ and S generally shows opposite temperature dependence regardless of being degenerately doped or non-degenerately doped.[25] The fact that σ and S show the same trend with temperature points to unconventional charge transport, a charge dynamics that cannot be described by the conventional free electron (Drude) model in band transport.

Mott's variable range hopping (VRH) model was developed to describe hopping conduction among localized states with energies concentrated within a narrow band near the Fermi level at relatively low temperatures.[26–28] The hopping process simultaneously takes into account thermally activated hopping over a potential energy barrier and phonon-assisted tunneling hopping between the localized states. The thermally activated hopping process is governed by the Boltzmann factor, $\exp(-W/k_BT)$, where W is the energy barrier between the localized state energies E_i and E_j. The tunneling probability is determined by the wavefunction overlap between localized states denoted as $\exp(-2\alpha R)$, where α^{-1} is the effective radius of wavefunction of the localization states. Taken together, the hopping probability is written

$$P_{ij} = \nu_0 \exp\left(-2\alpha R_{ij} - \frac{W}{k_BT}\right), \tag{1}$$

where R_{ij} is the distance between the two localized states and ν_0 is the phonon frequency gauging interactions of the hopping carrier and the lattice. It follows that the electrical conductivity then depends on temperature as $\sigma \sim \exp\{-1/T^{1/(d+1)}\}$, and the Seebeck coefficient as $S \sim T^{(d-1)/(d+1)}$, where d is the dimensionality of the system. This model effectively explains the abnormal temperature dependencies of σ and S.

Here, the thickness of the BP nanoribbons is $\sim$100 nm, and it is much higher than the size of wavefunction of the localization states ($\sim$25 nm in BP, Ref. 15) and their average distance. Hence, the 3D VRH model was adopted to fit the electric and thermoelectric transport (see the comparison of 2D and 3D VRH fitting in the supplementary material)

$$\sigma = \sigma_0 T^{-m} \exp\left(-\frac{A}{T^{1/4}}\right), \tag{2}$$

where σ_0 is a pre-factor and $m \approx 0.8$.[15,29,30] If A is written as $A = (T_0)^{1/4}$, T_0 is related to the density of states at the Fermi level $[D(E_F)]$ as $T_0 = 18.1\alpha^3/k_BD(E_F)$. In the same picture, the Seebeck coefficient is given as[31]

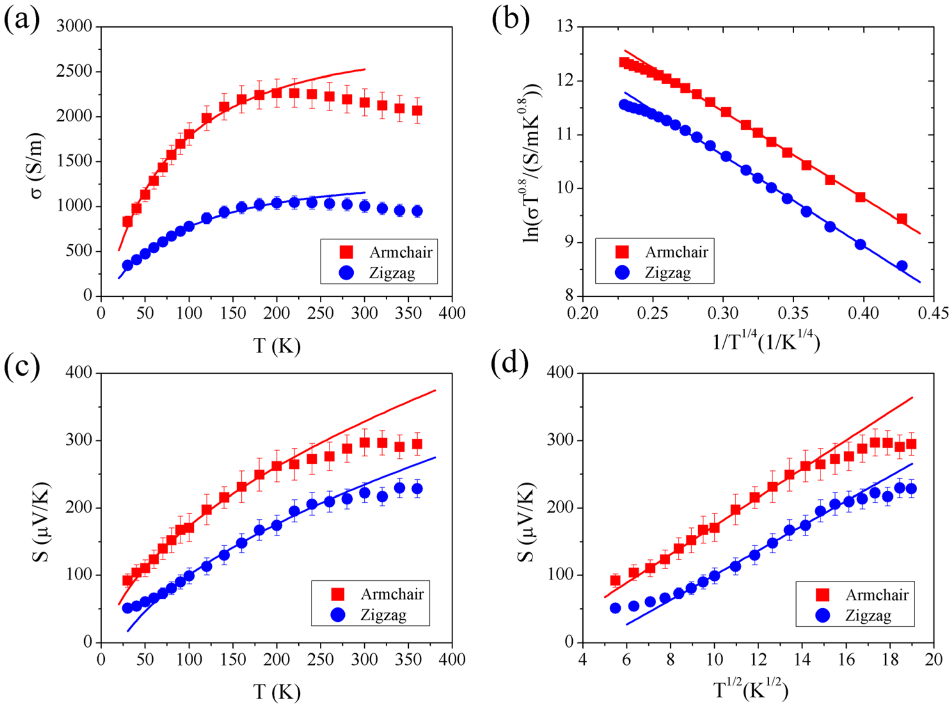

FIG. 3. Temperature dependence of electrical conductivity (σ) and Seebeck coefficient (S) of BP nanoribbons along the armchair and zigzag directions. Both the ribbons have thickness $\sim$100 nm. (a) σ versus T and (b) $\ln(\sigma T^{0.8})$ versus $1/T^{1/4}$; (c) S versus T and (d) S versus $T^{1/2}$. Solid lines are fitting results using 3D VRH model.

TABLE I. Fitting parameters of σ and S using the 3D VRH model. σ_0, A, and B are fitted values from σ and S, respectively; we calculated T_0, and estimated Density of states [$D(E)$] and dD/dE at the Fermi level, average hopping distance (R, 200 K) and hopping energy (W, 200 K), assuming $\alpha^{-1} = 25$ nm.

	σ_0 (10^7 S/mK$^{0.8}$)	A (K$^{1/4}$)	T_0 (10^4K)	B (μV/K$^{3/2}$)	R (200 K) (nm)	W (200 K) (meV)	D (E_F) (10^{17} eV^{-1} cm^{-3})	dD/dE (E = E_F) (10^{19} eV^{-2} cm^{-3})
Armchair	1.176	16.156	6.813	21.170	40.276	18.528	1.973	6.895
Zigzag	0.623	16.770	7.909	18.383	41.807	19.233	1.700	4.786

$$S = \frac{k_B}{2e}\left(\frac{3}{4\pi D(E_F)}\right)^{1/2}\left(\frac{2\alpha}{3}\right)^{3/2}\left(\frac{d\ln D(E)}{dE}\right)_{E=E_F}(k_BT)^{1/2}. \tag{3}$$

When temperature approaches zero, S scales as $S = BT^{1/2}$, where B is pre-factor.

The 3D VRH model was used to fit the data of σ and S for the armchair and zigzag nanoribbons, as shown in Figs. 3(b) and 3(d). The solid lines in Fig. 3 display the fitting results, and the fitting parameters are summarized in Table I. At $T \lesssim 200$ K, the VRH model shows good fitting with the data. σ deviates from the VRH prediction at $T \gtrsim 200$ K, probably due to thermal activated band transport, as the acceptor activation energy is ∼18 meV,[32] and acoustic phonons scattering grows to be competitive with the VRH process at high temperatures. When temperature goes below ∼50 K, the interactions among conducting electrons may need to be considered (the Efros model).[31] In this scenario, the Seebeck coefficient deviates from the Mott's picture and will approach a plateau with decreasing temperature, as observed in Fig. 3(c). Based on the parameters obtained from fitting σ and S, we also determine the density of states and slope of the density of states at the Fermi level, listed in Table I, assuming $\alpha^{-1} = 25$ nm (Ref. 15). The average hopping distance R is estimated from $R \sim 0.375(T_0/T)^{1/4}\alpha^{-1}$. At 200 K, the hopping distance R is ∼40.3 nm in armchair and ∼41.8 nm in the zigzag direction. The related average hopping energy W between localized states is calculated from $W \sim 3/(4\pi R^3 D(E_F))$, and at 200 K, it is ∼18.5 meV and 19.2 meV along the armchair and zigzag direction, respectively, which are consistent with the thermal energy at 200 K ($k_BT \sim 17$ meV). Although we do not have an independent way to analyze the anisotropy in these parameters in the VRH model, we take the conventional band transport picture as a comparison. In the band transport, the density of states is proportional to the electron effective mass $(m^*)^{3/2}$. BP has a lower effective mass for holes along the armchair than along the zigzag direction (by a factor of ∼0.16),[24] resulting in a lower (by a factor of ∼0.06) density of states in the armchair direction. We hypothesize that such trap states arise from native defects (atomic vacancies and interstitials) and impurities formed in the pristine BP flakes during the synthesis process. To independently test the validity of the VRH model, we artificially introduce more defects by irradiating the nanoribbons with 30 keV He^{2+} ion beams. The irradiation at this energy would allow the ions to completely go through the nanoribbon, leaving behind uniformly distributed atomic vacancies and interstitials. This is because the projected length of the ion irradiation is ∼340 nm (by SRIM simulation), deeper than the nanoribbon thickness. It is assumed that the atomic vacancies created by the irradiation are similar with the original defects for the electron hopping, and the irradiation increases the density, but not wavefunction, of the localized defect states. The electrical transports of the pristine and irradiated BP nanoribbons are shown in Fig. 4. It is expected that ion irradiation would create more atomic defects and trap states that reduce the average hopping distance R. The average hopping distance R (at 200 K) is estimated to be ∼35.9 nm after irradiated with a high dose of 1×10^{14} ions/cm^2, lower than that in the pristine sample (∼40.3 nm) in Fig. 4(a). The density of states of traps (∼3.1×10^{17} eV^{-1}cm^{-3}) at the Fermi level also becomes larger than in pristine sample (∼2.0×10^{17} eV^{-1}cm^{-3}) after the irradiation. According to Eq. (3), S is inversely proportional to the density of states. S is indeed reduced by irradiation at higher doses, as shown in Fig. 4(b) for S at 298 K, 198 K, and 78 K. Therefore, it is clear that the electrical and thermoelectric transports in BP are indeed dominated by hopping among defect states.

In conclusion, we quantify in-plane anisotropic electrical and thermoelectric transports in black phosphorus along its armchair and zigzag directions. In both directions, the electrical conductivity and Seebeck coefficient show the same trend with temperature, which cannot be explained by conventional band transport mechanism. We show that the

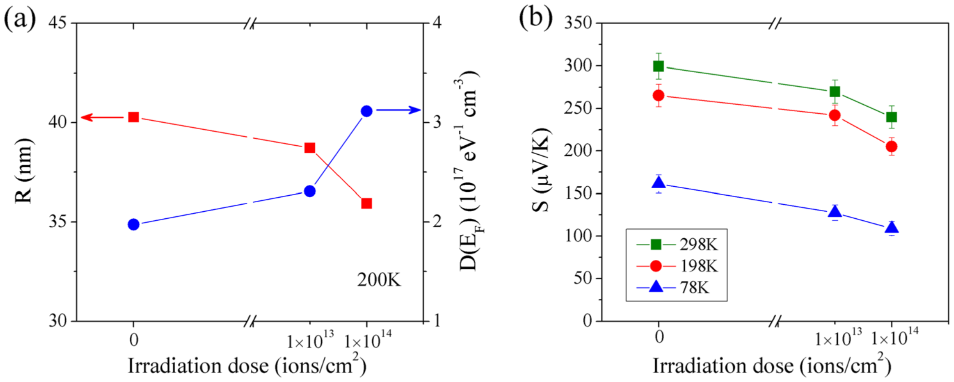

FIG. 4. Properties of a BP nanoribbon before and after He^{2+} irradiation. (a) Irradiation dose dependence of average hopping distance and density of states of traps at the Fermi level at 200 K. (b) Irradiation dose dependence of Seebeck coefficient at 298 K, 198 K, and 78 K.

transport in BP is governed by hopping of holes among trap states distributed within a narrow band in the bandgap, and the density of trap states can be increased with energetic particle irradiation. As the electrical and thermal[14] transport all show strong but different anisotropies in the basal plane, BP may serve as a 2D material platform for designing exotic routing of heat and charge flows at the microscale. The intrinsic anisotropy in BP may also add insights to the idea of "phonon-glass electron-crystal" (PGEC)[33] in thermoelectrics. The figure of merit might be further improved in BP by carrier doping or alloying with As,[34] making BP a potential material basis for high-performance thermoelectrics.

See supplementary material for methods of BP nanoribbons fabrication, details of measurements, and comparison of 2D and 3D VRH fitting.

This work was supported by the Electronic Materials Program at the Lawrence Berkeley National Laboratory, which is supported by the Office of Science, Office of Basic Energy Sciences, of the U.S. Department of Energy under Contract No. DE-AC02-05CH11231. H.C. and J.W. acknowledge support from the Tsinghua-Berkeley Shenzhen Institute (TBSI).

The authors declare no competing financial interest.

[1] L. E. Bell, "Cooling, heating, generating power, and recovering waste heat with thermoelectric systems," Science **321**, 1457–1461 (2008).

[2] G. J. Snyder and E. S. Toberer, "Complex thermoelectric materials," Nat. Mater. **7**, 105–114 (2008).

[3] M. S. Dresselhaus, G. Chen, M. Y. Tang, R. Yang, H. Lee, D. Wang, Z. Ren, J. P. Fleurial, and P. Gogna, "New directions for low-dimensional thermoelectric materials," Adv. Mater. **19**, 1043–1053 (2007).

[4] L. D. Hicks and M. S. Dresselhaus, "Thermoelectric figure of merit of a one-dimensional conductor," Phys. Rev. B **47**, 16631–16634 (1993).

[5] A. K. Geim and K. S. Novoselov, "The rise of graphene," Nat. Mater. **6**, 183–191 (2007).

[6] D. Jariwala, V. K. Sangwan, L. J. Lauhon, T. J. Marks, and M. C. Hersam, "Emerging device applications for semiconducting two-dimensional transition metal dichalcogenides," ACS Nano **8**, 1102–1120 (2014).

[7] L. Li, Y. Yu, G. J. Ye, Q. Ge, X. Ou, H. Wu, D. Feng, X. H. Chen, and Y. Zhang, "Black phosphorus field-effect transistors," Nat. Nanotechnol. **9**, 372–377 (2014).

[8] X. Ling, H. Wang, S. Huang, F. Xia, and M. S. Dresselhaus, "The renaissance of black phosphorus," Proc. Natl. Acad. Sci. U.S.A. **112**, 4523–4530 (2015).

[9] A. Castellanos-Gomez, "Black phosphorus: Narrow gap, wide applications," J. Phys. Chem. Lett. **6**, 4280–4291 (2015).

[10] E. Flores, J. R. Ares, A. Castellanos-Gomez, M. Barawi, I. J. Ferrer, and C. Sanchez, "Thermoelectric power of bulk black-phosphorus," Appl. Phys. Lett. **106**, 022102 (2015).

[11] Y. Saito, T. Iizuka, T. Koretsune, R. Arita, S. Shimizu, and Y. Iwasa, "Gate-tuned thermoelectric power in black phosphorus," Nano Lett. **16**, 4819–4824 (2016).

[12] H. Y. Lv, W. J. Lu, D. F. Shao, and Y. P. Sun, "Enhanced thermoelectric performance of phosphorene by strain-induced band convergence," Phys. Rev. B **90**, 085433 (2014).

[13] J. Zhang, H. J. Liu, L. Cheng, J. Wei, J. H. Liang, D. D. Fan, P. H. Jiang, L. Sun, and J. Shi, "High thermoelectric performance can be achieved in black phosphorus," J. Mater. Chem. C **4**, 991–998 (2016).

[14] S. Lee, F. Yang, J. Suh, S. Yang, Y. Lee, G. Li, H. S. Choe, A. Suslu, Y. Chen, C. Ko, J. Park, K. Liu, J. Li, K. Hippalgaonkar, J. J. Urban, S. Tongay, and J. Wu, "Anisotropic in-plane thermal conductivity of black phosphorus nanoribbons at temperatures higher than 100 K," Nat. Commun. **6**, 8573 (2015).

[15] S. J. Choi, B. K. Kim, T. H. Lee, Y. H. Kim, Z. Li, E. Pop, J. J. Kim, J. H. Song, and M. H. Bae, "Electrical and thermoelectric transport by variable range hopping in thin black phosphorus devices," Nano Lett. **16**, 3969–3975 (2016).

[16] J. Suh, K. M. Yu, D. Fu, X. Liu, F. Yang, J. Fan, D. J. Smith, Y. H. Zhang, J. K. Furdyna, C. Dames, W. Walukiewicz, and J. Wu, "Simultaneous enhancement of electrical conductivity and thermopower of Bi_2Te_3 by multifunctionality of native defects," Adv. Mater. **27**, 3681–3686 (2015).

[17] S. Lange, P. Schmidt, and T. Nilges, "Au3SnP7@black phosphorus: An easy access to black phosphorus," Inorg. Chem. **46**, 4028–4035 (2007).

[18] A. Castellanos-Gomez, L. Vicarelli, E. Prada, J. O. Island, K. L. Narasimha-Acharya, S. I. Blanter, D. J. Groenendijk, M. Buscema, G. A. Steele, J. V. Alvarez, H. W. Zandbergen, J. J. Palacios, and H. S. J. van der Zant, "Isolation and characterization of few-layer black phosphorus," 2D Mater. **1**, 025001 (2014).

[19] X. Ling, S. Huang, E. H. Hasdeo, L. Liang, W. M. Parkin, Y. Tatsumi, A. R. T. Nugraha, A. A. Puretzky, P. M. Das, B. G. Sumpter, D. B. Geohegan, J. Kong, R. Saito, M. Drndic, V. Meunier, and M. S. Dresselhaus, "Anisotropic electron-photon and electron-phonon interactions in black phosphorus," Nano Lett. **16**, 2260–2267 (2016).

[20] L. Shi, D. Li, C. Yu, W. Jang, D. Kim, Z. Yao, P. Kim, and A. Majumdar, "Measuring thermal and thermoelectric properties of one-dimensional nanostructures using a microfabricated device," J. Heat Transfer **125**, 881–888 (2003).

[21] J. Cao, W. Fan, H. Zheng, and J. Wu, "Thermoelectric effect across the metal-insulator domain walls in VO_2 microbeams," Nano Lett. **9**, 4001–4006 (2009).

[22] S. Lee, K. Hippalgaonkar, F. Yang, J. Hong, C. Ko, J. Suh, K. Liu, K. Wang, J. J. Urban, X. Zhang, C. Dames, S. A. Hartnoll, O. Delaire, and J. Wu, "Anomalously low electronic thermal conductivity in metallic vanadium dioxide," Science **355**, 371–374 (2017).

[23] J. Zhu, K. Hippalgaonkar, S. Shen, K. Wang, Y. Abate, S. Lee, J. Wu, X. Yin, A. Majumdar, and X. Zhang, "Temperature-gated thermal rectifier for active heat flow control," Nano Lett. **14**, 4867–4872 (2014).

[24] J. Qiao, X. Kong, Z. X. Hu, F. Yang, and W. Ji, "High-mobility transport anisotropy and linear dichroism in few-layer black phosphorus," Nat. Commun. **5**, 4475 (2014).

[25] H. J. Goldsmid, *Thermoelectric Refrigeration* (Plenum Press, New York, 1964).

[26] N. F. Mott and E. A. Davis, *Electronic Processes in Non-Crystalline Materials* (Clarendon Press, 1971).

[27] B. I. Shklovskii and A. L. Efros, *Electronic Properties of Doped Semiconductors* (Springer, London, 1984).

[28] T. E. Park, J. Suh, D. Seo, J. Park, D. Y. Lin, Y. S. Huang, H. J. Choi, J. Wu, C. Jang, and J. Chang, "Hopping conduction in p-type MoS_2 near the critical regime of the metal-insulator transition," Appl. Phys. Lett. **107**, 223107 (2015).

[29] S. Ghatak, A. N. Pal, and A. Ghosh, "Nature of electronic states in atomically thin MoS_2 field-effect transistors," ACS Nano **5**, 7707–7712 (2011).

[30] J. Wu, H. Schmidt, K. K. Amara, X. F. Xu, G. Eda, and B. Ozyilmaz, "Large thermoelectricity via variable range hopping in chemical vapor deposition grown single-layer MoS2," Nano Lett. **14**, 2730–2734 (2014).

[31] M. J. Burns and P. M. Chaikin, "Interaction effects and thermoelectric power in low-temperature hopping," J. Phys. C: Solid State Phys. **18**, L743–L749 (1985).

[32] Y. Akahama, S. Endo, and S. Narita, "Electrical properties of black phosphorus single crystals," J. Phys. Soc. Jpn. **52**, 2148–2155 (1983).

[33] G. A. Slack, in *CRC Handbook of Thermoelectrics*, edited by D. M. Rowe (CRC Press, Boca Raton, 1995), pp. 407–440.

[34] B. Liu, M. Kopf, A. N. Abbas, X. Wang, Q. Guo, Y. Jia, F. Xia, R. Weihrich, F. Bachhuber, F. Pielnhofer, H. Wang, R. Dhall, S. B. Cronin, M. Ge, X. Fang, T. Nilges, and C. Zhou, "Black arsenic-phosphorus: Layered anisotropic infrared semiconductor with highly tunable compositions and properties," Adv. Mater. **27**, 4423–4429 (2015).

Supplementary information

Variable range hopping electric and thermoelectric transport in anisotropic black phosphorus

Huili Liu[1,2], Hwan Sung Choe[2], Yabin Chen[2], Joonki Suh[2], Changhyun Ko[2], Sefaattin Tongay[3] and Junqiao Wu[1,2 *]

[1]Materials Sciences Division, Lawrence Berkeley National Laboratory, Berkeley, California 94720, USA.

[2]Department of Materials Science and Engineering, University of California, Berkeley, California 94720, USA.

[3]School for Engineering of Matter, Transport, and Energy, Arizona State University, Tempe, Arizona 85287, USA

METHODS

BP nanoribbons fabrication. BP bulk crystal was synthesized as reported before.[1] BP flakes were exfoliated onto SiO_2/Si substrate with PDMS (Polydimethylsiloxane) assisted, and the crystal orientation (armchair and zigzag direction) was identified using micro-Raman analysis. BP nanoribbons were fabricated by micro-patterned method with ~2um width and ~35um length using electron beam lithography (EBL). The flakes were spin coated by PMMA (Poly(methyl methacrylate), C4-950, 4000rpm) for 1 min and were baked at 180 °C for 5 mins. PMMA was exposed with desired patterns, followed by developing process using MIBK:IPA=1:3 developer for 1 min. Exposed BP was performed etching process via reactive ion etching method using mixed gas (90% SF_6 and 10% O_2, 60 sccm) for several seconds. After

PMMA removal with acetone and rinsed by isopropyl alcohol, BP nanoribbons were obtained. Ti/Au metal deposition process was conducted to improve both electrical and thermal contact for measurements. A second EBL process was applied to expose electrode windows on BP nanoribbons. Samples were performed Ar^+ milling (30-60s) to remove the oxidized layer on the surface, which form ohmic contacts between BP and deposited metals, and then Ti (10nm, deposition rate ~0.5Å/s) / Au (70nm, deposition rate ~1Å/s) metals were deposited by electron beam evaporation (CHA solution E-beam evaporator). Lift-off process was conducted in acetone for ~5mins with lightly shaking, followed by thoroughly rinsing with isopropyl alcohol. After that, BP nanoribbons were manually picked up using a sharp Tungsten needle (600 nm tip diameter, Cascade Microtech) assisted with the micro-manipulator probe station, and transferred onto a suspended-pad micro-device and aligned Ti/Au metal electrodes of BP nanoribbon onto the four electrodes on the suspended pads. Platinum was deposited to bond the Ti/Au and electrode of the pads using focused ion beam (FIB) technology (FEI Quanta). The SEM image of the device is shown in Fig. 2(h). After Pt deposition, the electrical contact of electrodes was verified by two probes method to demonstrate the linear I-V relationship (ohmic contact). The devices were also annealed at 373 K for one hour in vacuum chamber to improve the electrode bonding. BP crystal and samples were stored in dry N_2 flow atmosphere to prevent surface oxidation. The pristine BP nanoribbon samples (thickness~161nm) were irradiated using Zeiss ORION NanoFab Helium Ion Microscopy (HIM) with 30keV He^{2+} beam. The beam covered the whole nanoribbons and the accumulated irradiation doses were 1×10^{13} and 1×10^{14} ions/cm^2.

Measurements. The electrical property was measured using suspended-pad micro-devices. Pt electrodes on the suspended SiN_x pad were for four-probe electrical conductivity measurements, and Pt serpentine coils on each pad was designed for micro-heater or thermometer, providing joule heat on one pad (heater pad) and response the temperature variation on each pad. SiN_x arms supported the suspended pad, and coated with platinum for capturing electrical signals. When applying a DC current ($I_{DC} \sim$ 0-15uA) on the micro-heater (heater pad), the generated joule heat raises the heater pad temperature ΔT_h. The heat transfers to the other pad (sensor pad) and raises the temperature ΔT_s. An AC current (500 nA) is applied to respond to the resistance variation of the micro-heater or thermometer on each pad using Lock-in amplifier (Stanford SR810 or SR830). ΔT_h and ΔT_s can be obtained based on the resistance variation of Pt micro-heater or thermometer on the pad and Pt temperature coefficient of resistance, which was calibrated by the Pt coil resistance at each global temperature (100-360K with 20K interval and 30-100K with 10K interval, shown in Fig S1). Electrical conductance G was measured by the four-probe method with Pt electrodes on each pad. The length, width and thickness of the nanoribbons were measured using SEM and AFM. Seebeck coefficient was obtained by $S = -\Delta V/(\Delta T_h - \Delta T_s)$ with voltage (Keithley 6220A) gradient of nanoribbons and ΔT evaluated by resistance variation of Pt heater or thermometer on pads. The Seebeck coefficient of BP nanoribbons was calibrated with thermopower of platinum.[2] Measurements were performed under a low vacuum ($<10^{-6}$torr) with radiation shield in the chamber. The global temperature in the chamber was balanced with an external heater (Lakeshore 335) on the device holder and cryogenic compressor (Sumitomo). Data errors are estimated by sample dimensional errors and ΔT rising on each pad at global temperature.[3]

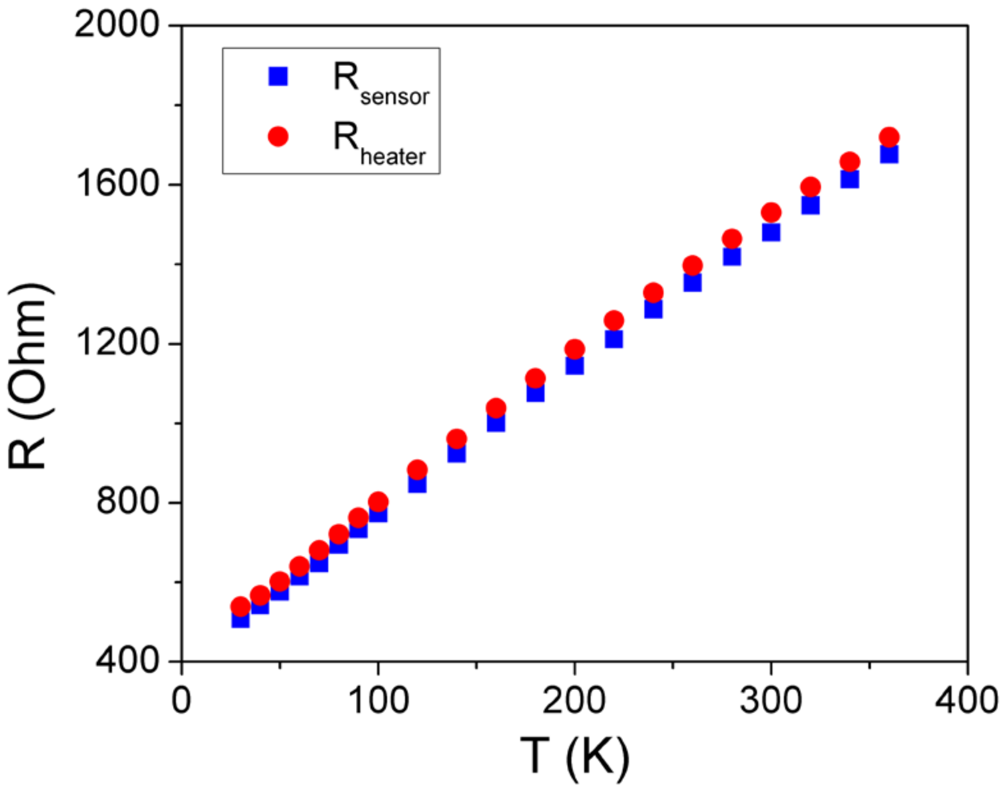

FIG. S1. Temperature dependence of resistance of Pt coils on heater and sensor pad.

REFERENCE

[1] S. Lee, F. Yang, J. Suh, S. Yang, Y. Lee, G. Li, H. S. Choe, A. Suslu, Y. Chen, C. Ko, J. Park, K. Liu, J. Li, K. Hippalgaonkar, J. J. Urban, S. Tongay, and J. Wu, "Anisotropic in-plane thermal conductivity of black phosphorus nanoribbons at temperatures higher than 100 K," Nat. Commun. **6**, 8573 (2015).

[2] J. P. Moore, R. S. Graves, "Absolute Seebeck coefficient of platinum from 80 to 340 K and the thermal and electrical conductivities of lead from 80 to 400 K," J. Appl. Phys. **44**, 1174-1178 (1973).

[3] L. Shi, D. Li, C. Yu, W. Jang, D. Kim, Z. Yao, P. Kim, and A. Majumdar, "Measuring thermal and thermoelectric properties of one-dimensional nanostructures using a microfabricated device," J. Heat Transfer **125**, 881-888 (2003).